Available online at www.sciencedirect.com

ScienceDirect

Procedia Structural Integrity 72 (2025) 97–104

Structural Integrity Procedia

www.elsevier.com/locate/procedia

12th Annual Conference of Society for Structural Integrity and Life (DIVK12)

Comparing Approaches for Predicting Critical Loads in 3D Printed Graphene-reinforced PLA Plates Containing Notches

Sergio Arrieta[a,*], Sergio Cicero[a], Marcos Sánchez[b], Juan Gil Calderón[a]

[a]*LADICIM (Laboratory of Materials Science and Engineering), Universidad de Cantabria, E.T.S. de Ingenieros de Caminos, Canales y Puertos, Av. Los Castros 44, Santander, 39005 Cantabria, Spain*

[b]*TECNALIA, Basque Research and Technology Alliance (BRTA), Mikeletegi Pasealekua 2, 20009 Donostia-San Sebastián, Gipuzkoa, Spain*

Abstract

This work provides a comparison of different methodologies that may be used to estimate critical loads in notched components. The use of 3D-printed composites in structural applications, surpassing the current prototyping application, requires the definition of safe and robust methodologies for the determination of critical loads. Considering that notches (corners, holes, grooves, etc.) are unavoidable in structural components, these stress risers affect the corresponding load-carrying capacity. This study compares the results obtained by applying two different methodologies: the Theory of Critical Distances (TCD) and the Averaged Strain Energy Density (ASED) criterion. Additionally, in the case of TCD, the Line Method, combined with Failure Assessment Diagrams, are used. These methodologies are employed to assess the critical loads in graphene-reinforced polylactic acid (PLA-Gr) plates manufactured by Fused Filament Fabrication with a fixed raster orientation at 45/−45. Furthermore, the plates contain two different notch types (U-notches and V-notches), and comprise various thicknesses (from 5 mm up to 20 mm) and ratios of notch length to plate width (a/W= 0.25 and a/W = 0.50). The comparison between the obtained experimental critical loads and the corresponding estimations derived from the application of the TCD and the ASED reveals that both approaches generate reasonably accurate results, with most of the predictions being safe.

© 2026 The Authors. Published by ELSEVIER B.V.
This is an open access article under the CC BY-NC-ND license (https://creativecommons.org/licenses/by-nc-nd/4.0)
Peer-review under responsibility of Aleksandar Sedmak, Branislav Djordjevic, Simon Sedmak Dr. Simon Sedmak, ssedmak@mas.bg.ac.rs, Innovation Center of Faculty of Mechanical Engineering, Belgrade, Serbia

Keywords: Fracture; Additive Manufacturing; Graphene; PLA; Notch

* Corresponding author. Tel.: +34-942-201705; fax: +34-942-201818.
E-mail address: sergio.arrieta@unican.es

2452-3216 © 2026 The Authors. Published by ELSEVIER B.V.
This is an open access article under the CC BY-NC-ND license (https://creativecommons.org/licenses/by-nc-nd/4.0)
Peer-review under responsibility of Aleksandar Sedmak, Branislav Djordjevic, Simon Sedmak Dr. Simon Sedmak, ssedmak@mas.bg.ac.rs, Innovation Center of Faculty of Mechanical Engineering, Belgrade, Serbia
10.1016/j.prostr.2025.08.079

1. Introduction

Fused Filament Fabrication (FFF) is a versatile additive manufacturing technique capable of producing complex 3D structures from a wide range of materials: polymers, metals, ceramics, composites, etc. The process involves extruding molten filament layer by layer to build the desired component. While FFF has been widely adopted for rapid prototyping, its application to load-bearing structural components has been limited due to inferior mechanical properties compared to traditional manufacturing methods like injection molding, extrusion, and blow molding.

To address this limitation and unlock the full potential of FFF, significant research efforts are under way to enhance the mechanical performance of 3D-printed materials and develop a deeper understanding of their behavior under various loading conditions (Ameri et al. (2020); Cantrell et al. (2017); Torabi et al. (2023)).

Additive manufacturing (AM) processes can result in the formation of stress-concentrating features within 3D-printed components. These features, which may include porosity, operational damage, or intentional design elements (e.g., holes, grooves, corners), can significantly influence the structural integrity of components. The presence of them can act as potential initiation sites for crack propagation, potentially leading to catastrophic failure or fatigue-related degradation. Conventional crack assessment methodologies, typically developed for sharp, crack-like defects, may overvalue the severity of rounded defects in AM components.

To improve the accuracy of fracture load predictions for notched components and reduce conservatism, several methods have been proposed in recent years. Two prominent approaches that have gained significant attention are the Theory of Critical Distances (TCD), by Taylor (2007), and the Average Strain Energy Density (ASED) criterion, by Berto and Lazzarin (2014). These methods have been successfully applied to analyze a wide range of materials and loading conditions. In addition, Failure Assessment Diagrams (FADs, BS7910, BSI (2019)) are a well-established tool for evaluating the structural integrity of components containing crack-like defects. However, their application is primarily limited to metallic components with crack-like defects. While some research has extended FAD assessments to non-metallic materials with cracks (Cicero et al. (2022); Fuentes et al. (2018)), the FADs, together with the TCD, can be used to assess FFF polymers with notches (Cicero et al. (2011); Cicero et al. (2023)).

This work justifies the use of both methodologies, the TCD and the ASED criterion, to generate reasonable accurate results. Also, the TCD combined with FADs are used, providing safe predictions.

Nomenclature

a	Notch size
AM	Additive Manufacture
ASED	Average Strain Energy Density
B	Specimen thickness
E	Young's modulus
FAD	Failure Assessment Diagram
FAL	Failure Assessment Line
FEA	Finite Element Analysis
FFF	Fused Filament Fabrication
K_I	Stress intensity factor
K_{mat}	Fracture thoughness
K_{mat}^N	Fracture toughness of notched materials
K_r	Fracture ratio of applied K_I to fracture toughness
L	Critical distance
L_r	Ratio of applied load to limit load
P	Applied load
P_{ASED}	Estimated critical load by ASED criterion
P_{est}	Estimated critical load
P_{exp}	Experimental critical load
P_{FEA}	Arbitrary tensile load in FEA (1 N)
P_L	Limit load

P_{FAD-LM}	Estimated critical load by FAD-LM
PM	Point Method
P_{PM}	Estimated critical load by PM
PLA-Gr	Graphene-reinforced polylactic acid
R_c	Critical radius
TCD	Theory of Critical Distances
W	Specimen width
$\overline{W}$	Average strain energy density
W_c	Critical average strain energy density
α	Notch-opening angle
ε_u	Strain under maximum load
ν	Poisson's ratio
σ_0	Inherent strength
ρ	Notch radius
σ_{max}	Maximum elastic stress at the notch tip
σ_u	Ultimate tensile strength
σ_y	Yield stress

2. Material

The material investigated in this study is FFF graphene-reinforced PLA (PLA-Gr, 1 wt.%), supplied as filaments for direct FFF printing. The tensile and fracture properties (Cicero et al. (2021)) are summarized in Table 1.

Table 1. Mechanical properties of FFF PLA-Gr material. Raster orientation 45/-45.

E (*MPa*)	σ_y (*MPa*)	σ_u (*MPa*)	ε_u (*%*)	L (*mm*)	K_{mat} ($MPam^{1/2}$)
3972	47.5	49.0	1.5	1.06	7.2

The printed plates were all manufactured by FFF using a Prusa i3 printer, following the same process defined for the tensile and fracture specimens used in the basic characterization of the material, thus with the following printing parameters: nozzle diameter 0.4 mm; nozzle temperature 200 ºC; bed temperature 75 ºC; printing rate 30 mm/s; infill level 100%; layer height 0.3 mm. In all cases, the specimens were printed with raster orientation 45/-45.

All notches were machined into the printed plates after the FFF process. A total of 39 plates were tested, incorporating two notch types (U-notches and V-notches), two nominal notch radii (0.9 mm and 1.3 mm), two nominal widths (60 mm and 120 mm), three thicknesses (5 mm, 10 mm, and 20 mm), and two notch length-to-width ratios (a/W = 0.25 and 0.50). Fig. 1 provides a schematic representation of the specimens, while Annex A details the actual geometrical dimensions, which may slightly deviate from the nominal values.

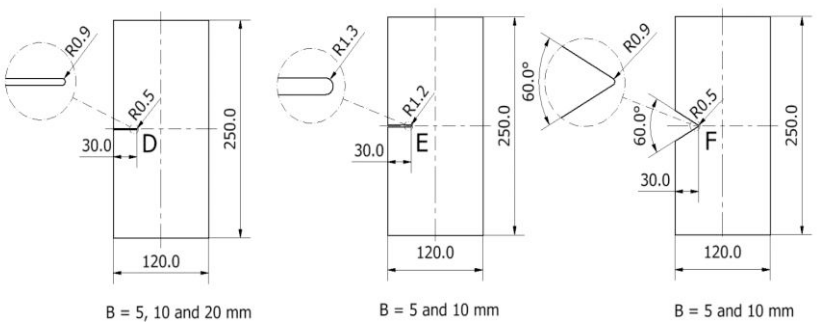

Fig. 1. Schematic of the tested specimens: U-notch and V-notch (Cicero et al. (2024)).

All notched plates were tested at a loading rate of 1 mm/min, consistent with the rate used in Cicero et al. (2021) for the basic tensile and fracture tests. The load-displacement curve was recorded for each test, and the corresponding critical load (P_{exp}) was determined (Table A.1). More details about the experimental programme in Cicero et al. (2023).

3. Methods

3.1. Theory of Critical Distances

The TCD is a collection of methodologies which, in the context of fracture mechanics, utilizes the critical distance parameter (L) in conjunction with the material's fracture toughness (K_{mat}). The Point Method (PM) has been widely validated for conventional materials with notch-type defects. However, its application to notched FFF materials, particularly those reinforced with graphene (Cicero et al. (2021)), has been limited.

The PM has demonstrated its ability to distinguish defects that affect load-bearing capacity from those that have no impact on the performance of fabricated components (Taylor (2004); Cicero et al. (2023)). As the simplest version of the TCD, it is based on the stress field at the notch tip. It is assumed that fracture occurs when the stress reaches a critical value (inherent strength, σ_0) at a distance L/2 from the defect tip, resulting in the following criterion:

$$\sigma(L/2) = \sigma_0 \tag{1}$$

The LM posits that fracture occurs when the average stress along a distance from the defect tip (2L) reaches the material's inherent strength (σ_0). Given the stress field at a crack tip, the LM expression is:

$$\frac{1}{2L}\int_0^{2L} \sigma(r)dr = \sigma_0 \tag{2}$$

In both cases, L is defined by equation:

$$L = \frac{1}{\pi}\left(\frac{K_{mat}}{\sigma_0}\right)^2 \tag{3}$$

where K_{mat} is the fracture toughness and σ_0 is the critical stress of the material. The latter is the maximum tensile strength (σ_u) in materials that behave elastic-linearly, while in non-linear materials, σ_0 requires calibration.

Once the PM parameters (L and σ_0) are determined, the stress field ahead of the notch tip must be defined. Here, FEA in linear-elastic conditions were conducted in ANSYS for each specimen with its specific geometry (see Table A.1 in Appendix A). By applying an arbitrary tensile load of P_{FEA} = 1 N, the stress field in the mid-plane of the fracture section was obtained, including the stress value at a distance of L/2 from the notch tip. The critical load was then calculated using proportionality. For a more detailed description, see Cicero et al. (2023).

3.2. Failure Assessment Diagrams

In the case of LM, it has been applied together with the Failure Assessment Diagrams (FAD-LM). Structural components with crack-like defects are typically assessed using structural integrity assessment procedures like BS7910 (BSI, 2019). These procedures rely on FADs to simultaneously analyze fracture and plastic collapse processes. This analysis involves two normalized parameters: K_r and L_r.

$$K_r = \frac{K_I}{K_{mat}} \tag{4}$$

$$L_r = \frac{P}{P_L} \tag{5}$$

where, the stress intensity factor (K_I), material fracture toughness (K_{mat}), applied load (P), and limit load (P_L) are used to evaluate components with crack-like defects.

The resulting assessment point on the FAD (K_r, L_r) is compared to the Failure Assessment Line (FAL). This curve separates safe and unsafe regions for a component with a crack-like defect. In this case, we use BS7910 Option 1 FAL from BSI (2019), which is a simplified approximation that provides a good balance between accuracy and simplicity. Here, the P_L values were obtained through linear interpolation between the plane stress and plane strain solutions provided by Anderson (2017).

Cicero et al. (2009) and Cicero et al. (2013) demonstrate that components with non-sharp defects (notches) exhibit an apparent fracture toughness (K_{mat}^N) that is higher than that of components with sharp cracks. The fracture behavior of notched materials can be analyzed using various criteria, including the TCD (through the Line Method, LM), integrated with FADs to develop structural integrity assessment criteria for components with notch-type defects:

$$K_r = \frac{K_I}{K_{mat}^N} = \frac{K_I}{K_{mat}\sqrt{1+\frac{\rho}{4L}}} \tag{6}$$

3.3. Average Strain Energy Density criterion

The Average Strain Energy Density (ASED) criterion (Lazzarin and Berto (2005); Berto and Lazzarin (2014)), states that brittle failure occurs when the average strain energy density ($\bar{W}$) within a control volume (or area in 2D cases) reaches a critical value (W_c), in elastic conditions. This can be mathematically expressed as:

$$\bar{W} = F(2\alpha) H\left(2\alpha, \frac{R_c}{\rho}\right) \frac{{\sigma_{max}}^2}{E} = W_c = \frac{{\sigma_u}^2}{2E} \tag{7}$$

$F(2\alpha)$ is a function of the notch opening angle (0.785 for $2\alpha = 0°$ - U-notches - and 0.662 for $2\alpha = 60°$), and H varies with both the notch geometry (2α, R_c/ρ) and the maximum elastic stress at the notch tip (σ_{max}). In a 2D case, the control volume becomes a circular sector with a critical radius R_c, which is influenced by the notch-opening angle (α). For U-notches, where $2\alpha = 0$ (see Fig. 4), the following expressions for R_c has been derived in Yosibash et al. (2004):

$$R_c = \frac{(1+\upsilon)(5-8\upsilon)}{4\pi}\left(\frac{K_{mat}}{\sigma_u}\right)^2 \qquad \textit{Plane strain} \tag{8}$$

$$R_c = \frac{(5-3\upsilon)}{4\pi}\left(\frac{K_{mat}}{\sigma_u}\right)^2 \qquad \textit{Plane stress} \tag{9}$$

where K_{mat} is the fracture toughness, σ_u is the ultimate tensile strength, and ν is Poisson's ratio.

Based on the failure criterion established by ASED the maximum stress at the notch tip can be deduced from the calculated H values and the material's mechanical properties:

$$\sigma_{max,\,ASED} = \sqrt{\frac{W_c^* \cdot E}{F(2\alpha)\cdot H\left(2\alpha, \frac{R_c^*}{\rho}\right)}} \tag{10}$$

Therefore, the application of this approach requires the definition of the maximum principal stress at the notch tip. The maximum principal stress at the notch tip has been determined for an external tensile load of P_{FEA} = 1N. Subsequently, the critical load is determined proportionally by applying equation (11):

$$P_{ASED} = \frac{\sigma_{max,\,ASED}}{\sigma_{max,\,FEA}}\ P_{FEA} \tag{11}$$

4. Results and discussion

Table A.1 in Appendix A presents the experimental and the predicted critical loads obtained from the three approaches, while Figures 2 and 3 compare the different results through the resulting P_{est}/P_{exp} ratios. Here, the ASED criterion provides the more accurate results, with most data points falling within a ±20% dispersion.

For TCD-based methods (PM and FAD-LM), approximately 35% of data points deviate more than ±20% from the expected values. While FAD-LM consistently underestimates fracture loads, the PM method overestimates them, particularly for G300 specimens.

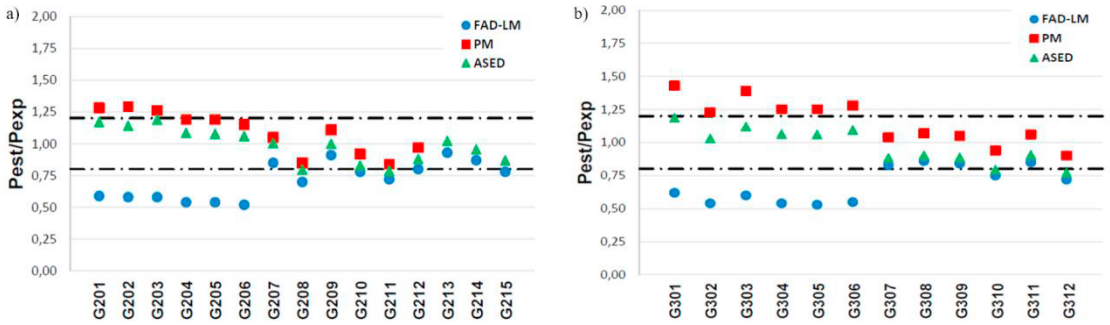

Fig. 2. Comparison of estimated and experimental fracture loads: a) G201-G215 (U-notch, ρ = 0.9 mm); b) G301-G312 (U-notch, ρ = 1.3 mm).

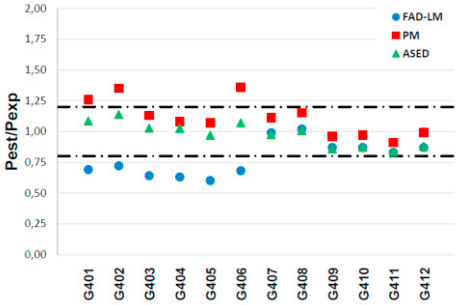

Fig. 3. Comparison of estimated and experimental fracture loads for specimens G401-G412 (V-notch and ρ = 0.9 mm).

5. Conclusions

In this work, three different methodologies (TCD-PM, FAD-LM and ASED) are applied to estimate the fracture loads in a total of 39 FFF PLA-Gr specimens with different types of notches. Applying TCD and FADs to U and V-type notched specimens, results are safe and conservative; the PM method accurately predicted experimental critical loads, although with an average overestimation of 11%, which might be attributed to the calibration procedure for L and σ_0 parameters using SENB data reported in Cicero et al. (2021); finally, the conventional linear elastic ASED criterion provided accurate predictions of critical loads, with experimental P_{ASED}/P_{exp} values falling within ±20% and an average underestimation of 2.4%. This accuracy can be attributed to the linear elastic behavior of graphene-reinforced PLA. However, for materials with nonlinear behavior, the effectiveness of this criterion might be compromised. A moderate effect of specimen thickness and notch size is also observed (a/W = 0.25).

Acknowledgements

This publication is part of the project "Comportamiento en fractura y efecto entalla en compuestos de matriz termoplástica obtenidos por fabricación aditiva, PID2021-122324NB-I00" funded by MCIN/AEI/10.13039 /501100011033/FEDER "Una manera de hacer Europa".

Appendix A. Collection of experimental and estimated critical loads

Details in Cicero et al. (2023), Cicero et al. (2024)) and Sánchez et al. (2023).

Table A.1. Experimental and predicted critical loads. U-notched specimens: G201-G3012; V-notched specimens: G401-412.

Spec.	a (*mm*)	W (*mm*)	a/W	ρ (*mm*)	B (*mm*)	P_{exp} (*KN*)	PM		FAD-LM				ASED	
							P_{PM} (*KN*)	P_{PM}/P_{exp}	Kr	Lr	P_{FAD-LM} (*KN*)	P_{FAD-LM}/P_{exp}	P_{ASED} (*KN*)	P_{ASED}/P_{exp}
G201	30.60	60.51	0.51	0.86	4.85	3.87	4.96	1.28	1.49	1.29	2.30	0.59	4.54	1.17
G202	30.84	60.38	0.51	0.91	4.88	3.86	4.99	1.29	1.51	1.31	2.25	0.58	4.42	1.15
G203	30.73	60.50	0.51	0.83	4.85	3.89	4.93	1.27	1.52	1.31	2.25	0.58	4.62	1.19
G204	30.66	60.46	0.51	0.87	10.02	8.52	10.15	1.19	1.60	1.37	4.60	0.54	9.26	1.09
G205	30.59	60.46	0.51	0.88	9.96	8.54	10.15	1.19	1.60	1.38	4.60	0.54	9.21	1.08
G206	30.83	60.49	0.51	0.86	9.98	8.76	10.11	1.15	1.67	1.43	4.60	0.53	9.29	1.06
G207	31.02	120.36	0.26	0.81	4.96	10.55	11.09	1.05	1.07	0.66	9.00	0.85	10.61	1.01
G208	30.34	120.31	0.25	0.83	4.98	13.15	11.19	0.85	1.29	0.80	9.20	0.70	10.46	0.80
G209	30.58	120.20	0.25	0.89	4.97	10.14	11.28	1.11	1.00	0.63	9.20	0.91	10.14	1.00
G210	31.02	120.36	0.26	0.89	10.14	24.43	22.40	0.92	1.20	0.74	19.00	0.78	20.28	0.83
G211	30.92	120.43	0.26	0.84	10.13	26.41	22.28	0.84	1.30	0.80	19.00	0.72	20.79	0.79
G212	31.06	120.48	0.26	0.88	10.00	23.07	22.36	0.97	1.15	0.71	18.50	0.80	20.33	0.88
G213	31.08	120.43	0.26	0.88	20.17	39.90	45.06	1.13	0.98	0.57	37.00	0.93	40.82	1.02
G214	31.25	120.62	0.26	0.89	20.05	42.56	45.08	1.06	1.06	0.62	37.00	0.87	40.71	0.96
G215	30.83	120.63	0.26	0.87	20.14	47.30	45.06	0.95	1.16	0.68	37.00	0.78	41.16	0.87
G301	30.85	60.48	0.51	1.24	4.86	3.69	5.26	1.43	1.39	1.23	2.30	0.62	4.38	1.19
G302	30.98	60.40	0.51	1.24	4.91	4.29	5.26	1.23	1.63	1.44	2.30	0.54	4.42	1.03
G303	30.91	60.54	0.51	1.26	4.77	3.80	5.29	1.39	1.47	1.30	2.30	0.61	4.27	1.12
G304	30.85	60.47	0.51	1.26	9.96	8.63	10.75	1.25	1.59	1.38	4.65	0.54	9.17	1.06
G305	31.19	60.55	0.52	1.27	9.92	8.60	10.77	1.25	1.62	1.41	4.60	0.53	9.12	1.06
G306	30.95	60.47	0.51	1.25	9.93	8.40	10.73	1.28	1.56	1.36	4.60	0.55	9.20	1.10
G307	30.62	120.32	0.25	1.26	4.88	11.51	11.95	1.04	1.12	0.71	9.60	0.83	10.19	0.89
G308	30.93	120.30	0.26	1.27	4.92	11.21	11.97	1.07	1.09	0.69	9.60	0.86	10.15	0.91
G309	30.92	120.42	0.26	1.26	4.94	11.46	12.00	1.05	1.11	0.70	9.60	0.84	10.17	0.89
G310	31.02	120.25	0.26	1.27	9.96	25.37	23.79	0.94	1.22	0.77	19.00	0.75	20.19	0.80
G311	31.04	120.33	0.26	1.26	9.93	22.38	23.77	1.06	1.08	0.69	19.00	0.85	20.30	0.91
G312	31.08	120.43	0.26	1.26	9.93	26.31	23.78	0.90	1.27	0.80	19.00	0.72	20.30	0.77
G401	27.03	60.56	0.45	1.25	4.76	4.27	5.40	1.26	1.27	1.10	2.95	0.69	4.64	1.09
G402	26.87	60.54	0.44	1.05	4.80	4.09	5.54	1.35	1.21	1.03	2.95	0.72	4.65	1.14
G403	26.99	60.49	0.45	0.89	4.83	4.58	5.16	1.13	1.38	1.16	2.95	0.64	4.71	1.03
G404	26.95	60.60	0.44	0.65	9.92	9.56	10.31	1.08	1.43	1.15	6.00	0.63	9.79	1.02
G405	26.92	60.55	0.44	0.93	9.99	10.04	10.74	1.07	1.45	1.20	6.00	0.60	9.73	0.97

G406	26.93	60.58	0.44	0.87	9.92	8.76	11.96	1.37	1.28	1.06	6.00	0.68	9.37	1.07
G407	26.95	120.24	0.22	1.07	4.89	10.65	11.80	1.11	0.93	0.61	10.50	0.99	10.38	0.97
G408	26.50	120.26	0.22	1.15	4.83	10.30	11.84	1.15	0.89	0.59	10.50	1.02	10.36	1.01
G409	26.80	120.33	0.22	1.01	4.86	12.05	11.56	0.96	1.06	0.69	10.50	0.87	10.35	0.86
G410	26.96	120.46	0.22	0.97	9.94	24.25	23.42	0.97	1.05	0.68	21.00	0.87	21.12	0.87
G411	26.92	120.29	0.22	0.89	9.95	25.32	23.13	0.91	1.11	0.71	21.00	0.83	21.13	0.83
G412	26.87	120.53	0.22	1.05	9.95	24.10	23.99	1.00	1.03	0.68	21.00	0.87	21.16	0.88

References

Ameri, B., Taheri-Behrooz, F., Aliha, M.R.M., 2020. “Fracture Loads Prediction of the Modified 3D-Printed ABS Specimens under Mixed-Mode I/II Loading.” Engineering Fracture Mechanics 235: 107181. https://linkinghub.elsevier.com/retrieve/pii/S0013794420307645

Anderson, T. L., 2017. Fracture Mechanics: Fundamentals and Applications. 4th ed. Boca Raton: CRC Press

Berto, F., Lazzarin, P., 2014. “Recent Developments in Brittle and Quasi-Brittle Failure Assessment of Engineering Materials by Means of Local Approaches.” Materials Science and Engineering R: Reports 75(1): 1–48

British Standards Institution, 2019. “BS 7910:2019, Guide to Methods for Assessing the Acceptability of Flaws in Metallic Structures.”

Cantrell, J.T., Rohde, S., Damiani, D., Gurnani, R., DiSandro, L., Anton, J., Young, A., Jerez, A., Steinbach, D., Kroese, C., et al., 2017. “Experimental Characterization of the Mechanical Properties of 3D-Printed ABS and Polycarbonate Parts.” Rapid Prototyping Journal 23(4): 811–24. https://www.emerald.com/insight/content/doi/10.1108/RPJ-03-2016-0042/full/html

Cicero, S., Arrieta, S., Sanchez, M., 2024. “Structural Integrity Evaluation of 3D Printed Graphene-Reinforced PLA Notched Plates Using Failure Assessment Diagrams.” In Volume 4: Materials & Fabrication, American Society of Mechanical Engineers. https://asmedigitalcollection.asme.org/PVP/proceedings/PVP2024/88506/V004T06A033/1209553

Cicero, S., Arrieta, S., Sanchez, M., Castanon-Jano, L., 2023. “Analysis of Additively Manufactured Notched PLA Plates Using Failure Assessment Diagrams.” Theoretical and Applied Fracture Mechanics 125: 103926

Cicero, S, Arrieta, S., Sánchez, M., Castanon-Jano, L., 2024. “Using the Point Method to Estimate Failure Loads in 3D Printed Graphene-Reinforced PLA Notched Plates.” Journal of Physics: Conference Series 2692(1): 012043

Cicero, S., Gutiérrez-Solana, F., Horn, A. J., 2009. “Experimental Analysis of Differences in Mechanical Behaviour of Cracked and Notched Specimens in a Ferritic-Pearlitic Steel: Considerations about the Notch Effect on Structural Integrity.” Engineering Failure Analysis 16(7): 2450–66

Cicero, S., Madrazo, V., Carrascal, I. A., Cicero, R., 2011. “Assessment of Notched Structural Components Using Failure Assessment Diagrams and the Theory of Critical Distances.” Engineering Fracture Mechanics 78(16): 2809–25

Cicero, S., Madrazo, V., García, T., Cuervo, J., Ruiz, E., 2013. “On the Notch Effect in Load Bearing Capacity, Apparent Fracture Toughness and Fracture Mechanisms of Polymer PMMA, Aluminium Alloy Al7075-T651 and Structural Steels S275JR and S355J2.” Engineering Failure Analysis 29: 108–21. https://linkinghub.elsevier.com/retrieve/pii/S1350630712002567

Cicero, S., Martínez-Mata, V., Castanon-Jano, L., Alonso-Estebanez, A., Arroyo, B., 2021. “Analysis of Notch Effect in the Fracture Behaviour of Additively Manufactured PLA and Graphene Reinforced PLA.” Theoretical and Applied Fracture Mechanics 114

Cicero, S., Martínez-Mata, V., Sánchez, M., Arrieta, S., 2022. “Analysis of Additively Manufactured PLA Containing Notches Using Failure Assessment Diagrams.” Procedia Structural Integrity 42: 18–26. https://linkinghub.elsevier.com/retrieve/pii/S2452321622005583

Cicero, S., Sánchez, M., Arrieta, S., 2023. “Predicting Critical Loads in Fused Deposition Modeling Graphene-Reinforced PLA Plates Containing Notches Using the Point Method.” Polymers 15(18): 3797. https://www.mdpi.com/2073-4360/15/18/3797

Cicero, S., Sánchez, M., Martínez-Mata, V., Arrieta, S., Arroyo, B., 2022. “Structural Integrity Assessment of Additively Manufactured ABS, PLA and Graphene Reinforced PLA Notched Specimens Combining Failure Assessment Diagrams and the Theory of Critical Distances.” Theoretical and Applied Fracture Mechanics 121: 103535. https://linkinghub.elsevier.com/retrieve/pii/S0167844222002798

Creager, M., Paris, P. C., 1967. “Elastic Field Equations for Blunt Cracks with Reference to Stress Corrosion Cracking.” International Journal of Fracture Mechanics 3(4): 247–52

Fuentes, J.D., Cicero, S., Ibáñez-Gutiérrez, F. T., Procopio, I., 2018. “On the Use of British Standard 7910 Option 1 Failure Assessment Diagram to Non-metallic Materials.” Fatigue & Fracture of Engineering Materials & Structures 41(1): 146–58

Lazzarin, P., Berto, F., 2005. “Some Expressions for the Strain Energy in a Finite Volume Surrounding the Root of Blunt V-Notches.” International Journal of Fracture 135(1–4): 161–85. http://link.springer.com/10.1007/s10704-005-3943-6

Sánchez, M., Arrieta, S., Cicero, S., 2023. “Fracture Load Estimations for U-Notched and V-Notched 3D Printed PLA and Graphene-Reinforced PLA Plates Using the ASED Criterion.” Frattura ed Integrità Strutturale 17(66): 322–38

Taylor, D., 2004. “Predicting the Fracture Strength of Ceramic Materials Using the Theory of Critical Distances.” Engineering Fracture Mechanics 71(16–17): 2407–16. https://linkinghub.elsevier.com/retrieve/pii/S0013794404000219

Taylor, D., 2007. The Theory of Critical Distances: A New Perspective in Fracture Mechanics The Theory of Critical Distances. Elsevier

Torabi, A.R., Shahbaz, S., Ayatollahi, M. R., 2023. “Fracture Assessment of U-Notched Diagonally Loaded Square Plates Additively Manufactured from ABS with Different Raster Orientations.” Engineering Structures 292: 116537

Yosibash, Z., Bussiba, A., Gilad, I., 2004. “Failure Criteria for Brittle Elastic Materials.” International Journal of Fracture 125(3–4): 307–33